Supplemental Material: Photo-induced electron pairing in a driven cavity

H. Gao,[1,*] **F. Schlawin**,[1,†] **Michele Buzzi**,[2,‡] **Andrea Cavalleri**,[1,2,§] and **D. Jaksch**[1,¶]

[1] *Clarendon Laboratory, University of Oxford, Parks Road, Oxford OX1 3PU, United Kingdom*

[2] *Max Planck Institute for the Structure and Dynamics of Matter, Hamburg, Germany*

[*] hongmin.gao@physics.ox.ac.uk

[†] frank.schlawin@physics.ox.ac.uk

[‡] michele.buzzi@mpsd.mpg.de

[§] andrea.cavalleri@mpsd.mpg.de

[¶] dieter.jaksch@physics.ox.ac.uk

I. DERIVATION OF THE LIGHT-MATTER INTERACTION HAMILTONIAN: COULOMB GAUGE

In this section we outline how to derive the light-matter Hamiltonian. We base our discussion on the geometry of Fig. 1 in the main text. Following the approach in Ref. [S1], we include both the mobile electrons and the positively charged background, whose charge density centers around and neutralises the 2D plane of the mobile electrons. We assume that the background atoms move so slowly that their centres of mass are fixed. Since the atoms from the background material can have electric dipole moments, we model the total displacement field of the background material alone as $\boldsymbol{D}_{\rm bg} = \boldsymbol{D}_{static} + \boldsymbol{P}$, where $\boldsymbol{\nabla}\cdot\boldsymbol{D}_{static} = \rho_{\rm bg}(\boldsymbol{r}) = \sum_{j\in{\rm bg}} Q_j\delta(\boldsymbol{r}-\boldsymbol{r}_j)$ and the bulk polarization, $\boldsymbol{P}(\boldsymbol{r},t) = \epsilon_0\chi_{\rm bg}\mathbf{E}(\boldsymbol{r},t)$ where $\mathbf{E}$ is the net electric field strength at $\boldsymbol{r}$ and time t, ϵ_0 is the vacuum permittivity. We have expressed the static background charge distribution as a sum over the collection of stationary particles $\{j\}$, with charge $\{Q_j\}$ at position $\{\boldsymbol{r}_j\}$. We have also approximated this polarization by a phenomenological polarizability constant $\chi_{\rm bg}$, that is independent of position and frequency.

To derive the full light-matter Hamiltonian, we start from the usual Lagrangian formulation of charged particles interacting with electromagnetic field with background polarizability incorporated,

$$L = \sum_{j=1}^{N}\Big[\frac{1}{2}m_j\dot{\boldsymbol{r}}_j^2 + Q_j\dot{\boldsymbol{r}}\cdot\mathbf{A}(\boldsymbol{r}_j,t) - Q_j\phi(\boldsymbol{r}_j,t)\Big] + \frac{\epsilon_0}{2}\int {\rm d}^3\boldsymbol{r}\,\Big[\epsilon_r\mathbf{E}^2(\boldsymbol{r},t) - c^2\mathbf{B}^2(\boldsymbol{r},t)\Big], \quad \text{(S1)}$$

where m_j is the mass of particle j (either a mobile electron or a stationary background charged atom) with electric charge Q_j located at $\boldsymbol{r}_j$, where the net electrical potential is $\phi(\boldsymbol{r}_j,t)$ and the vector potential is $\mathbf{A}$. $\dot{\boldsymbol{r}}$ means the time derivative of $\boldsymbol{r}$. c is the speed of light in vacuum, $\epsilon_r = 1+\chi_{\rm bg}$. The first term of Eq. (S1) describes light-matter interaction while the second term is the light field in the medium formed by the background atoms.

Following the usual procedures outlined in Ref. [S1], we obtain the Hamiltonian in Coulomb gauge, where the vector potential $\mathbf{A}$ is the transverse field whereas ϕ is the longitudinal field.

$$H = \sum_{j=1}^{N}\Big[\frac{(\boldsymbol{p}_j - Q_j\mathbf{A}(\boldsymbol{r}_j,t))^2}{2m_j} + \frac{1}{2}Q_j\phi(\boldsymbol{r}_j,t)\Big] + \frac{\epsilon_0}{2}\int {\rm d}^3\boldsymbol{r}\,\Big[\epsilon_r\dot{\mathbf{A}}^2 - \mathbf{A}\cdot\nabla^2\mathbf{A}\Big] \quad \text{(S2)}$$

Here $\boldsymbol{p}_j$ is the conjugate momentum of $\boldsymbol{r}_j$ and we assume the fields decay to zero at the

boundaries infinitely far away. We also have $\phi(\boldsymbol{r}) = \sum_j \frac{Q_j}{4\pi\epsilon_0\epsilon_r|\boldsymbol{r}-\boldsymbol{r}_j|}$.

We note that calculations may also be done in a different gauge and for calculations involving resonant coupling the dipolar gauge is better suited [S2], but leads to a more complicated interaction terms. In this work, we keep away from resonance (see Sec. II) so the Coulomb gauge is appropriate and the resulting interaction particularly simple.

The particle index above runs over both mobile electrons and background particles. Since the latter are treated as stationary, their kinetic energies are ignored and their positions are treated as parameters instead of variables. Thus, the Coulomb energy between them is a constant and the Coulomb energy between electrons and background atoms forms a static potential $V_b(\boldsymbol{r})$ for the electrons which confines the mobile electron tightly in the 2D plane at $z = \pi/2q_L$, where q_L refers to laser photon wavevector that we fix to lie along z-axis. Thus, the total potential energy of the electron j due to the background charges is $V_{bg}(\boldsymbol{r}_j) = -eV_b(\boldsymbol{r}_j)$, where $-e$ is the electron charge. The Hamiltonian [Eq. (S2)] becomes,

$$H = \sum_{j\in e^-}\Big[\frac{\left(\boldsymbol{p}_j + e\mathbf{A}(\boldsymbol{r}_j,t)\right)^2}{2m} + V_{bg}(\boldsymbol{r}_j)\Big] + \frac{1}{2}\sum_{\substack{j\neq k\\ j,k\in e^-}}\frac{e^2}{4\pi\epsilon_0\epsilon_r|\boldsymbol{r}_j-\boldsymbol{r}_k|} + \frac{\epsilon_0}{2}\int \mathrm{d}^3\boldsymbol{r}\,\Big[\epsilon_r\dot{\mathbf{A}}^2 - \mathbf{A}\cdot\nabla^2\mathbf{A}\Big]. \tag{S3}$$

Here m is the bare electron mass.

Following Ref. [S1], the vector potential $\mathbf{A}$ satisfies the equation

$$\left(\nabla^2 - \frac{\epsilon_r}{c^2}\frac{\partial^2}{\partial t^2}\right)\mathbf{A}(\boldsymbol{r},t) = -\mu_0\left(\sum_j Q_j\boldsymbol{v}_j\delta(\boldsymbol{r}-\boldsymbol{r}_j) - \epsilon_0\epsilon_r\boldsymbol{\nabla}\frac{\partial\phi}{\partial t}\right) \tag{S4}$$

Here $\boldsymbol{v}_j$ is the velocity of particle j (which is only non-zero for mobile electrons).

Since we are considering a driven cavity system, we write the solution as a mode expansion of the EM field plus the driving transverse field whose vector potential oscillates with angular frequency ω_L (from the driving laser) and amplitude $\mathbf{A}_d$ and which we treat as classical,

$$\mathbf{A}(\boldsymbol{r},t) = \sum_q \mathcal{A}_q\mathcal{C}_q(t)\boldsymbol{u}_q(\boldsymbol{r}) + \mathbf{A}_d\sin(q_Lz - \omega_Lt). \tag{S5}$$

$\mathbf{u}_q(\boldsymbol{r})$ are transverse photon mode functions that form a complete and orthonormal basis and satisfy

$$\left(\nabla^2 + \frac{\epsilon_r\omega_q^2}{c^2}\right)\boldsymbol{u}_q(\boldsymbol{r}) = 0\ , \tag{S6}$$

where ω_q is the frequency the cavity mode labelled q oscillate at. We consider that all the light modes are confined inside a box with periodic boundary conditions whose size $\mathcal{V}$ tends to infinity. We categorise the light modes into the cavity mode and the environment modes.

a. Cavity modes The split-ring THz cavity covers only a small area. Hence, we model the cavity to support a single mode (that is the lowest frequency (or fundamental) mode supported by the cavity) whose electric field points in the xy-plane parallel to the laser polarization and its strength is modulated by the lowest order standing wave in the perpendicular direction to the electric field with nodes at the boundaries, as shown in Fig. 1 of the main text. Thus the mode function is real, $\boldsymbol{u}_c(\mathbf{r}) = \sqrt{\frac{2}{\mathcal{V}_c}}\cos(q_0 x)$, where $q_0 = \omega_c\sqrt{\epsilon_r}/c$ as presented in the main text.

b. Environment modes It is clear that the cavity modes are only a small fractions of all the light modes inside the periodic box we used to define the light modes. Most of the other modes don't 'see' the mirrors as they are of different frequencies from the cavity modes or they are travelling at such large angles from cavity axis. We treat them as the environment modes. We use complex mode functions $\mathbf{u}_{q_e\equiv\{\mathbf{q}_e,s\}}$ (with $\mathbf{u}^*_{q_e} = \mathbf{u}_{-q_e}$) that describe travelling plane waves for the environment modes whose indices can be interpreted as momentum ($\mathbf{q}_e$) and polarization labels (s) for the modes.

With this mode decomposition, we can rewrite the free EM field the Hamiltonian as

$$H_{\text{free EM field}} = \frac{\epsilon_0}{2}\sum_{q\in\{c,q_e\}}\mathcal{A}_q^2(1+\chi_{\text{bg}})\Big[\pi_q\pi_{-q} + \omega_q^2\mathcal{C}_q\mathcal{C}_{-q}\Big] = \frac{1}{2}\sum_q\Big[\pi_q\pi_{-q} + \omega_q^2\mathcal{C}_q\mathcal{C}_{-q}\Big], \quad \text{(S7)}$$

where $\pi_q = \dot{\mathcal{C}}_{-q}$ is the conjugate momentum for $\mathcal{C}_q$, $\mathcal{C}_{-q} = \mathcal{C}_q$ when q refers to the cavity mode and we introduce the normalisation constant $\mathcal{A}_q = \frac{1}{\sqrt{\epsilon_0(1+\chi_{\text{bg}})}} \equiv \frac{1}{\sqrt{\epsilon_0\epsilon_r}}$.

Combine the above discussion with Eq. (S3), we arrive at the full Hamiltonian,

$$H = \sum_{j\in e^-}\Big[\frac{\Big(\boldsymbol{p}_j + e\Big[\frac{1}{\sqrt{\epsilon_0\epsilon_r}}\sum_q \mathcal{C}_q(t)\boldsymbol{u}_q(\boldsymbol{r}_j) + \mathbf{A}_d\cos(\omega_L t)\Big]\Big)^2}{2m} + V_{bg}(\boldsymbol{r}_j)\Big] + \frac{1}{2}\sum_{\substack{j\neq k\\ j,k\in e^-}}\frac{e^2}{4\pi\epsilon_0\epsilon_r|\boldsymbol{r}_j - \boldsymbol{r}_k|} + \frac{1}{2}\sum_q\Big[\pi_q\pi_{-q} + \omega_q^2\mathcal{C}_q\mathcal{C}_{-q}\Big]. \quad \text{(S8)}$$

We obtain the Hamiltonian for the quantum system through canonical quantisation of the above classical Hamiltonian.

A. Electron Hamiltonian

The electron field can be quantised by imposing the commutation relation

$$\big[(\boldsymbol{r}_j)_l, (\boldsymbol{p}_k)_m\big] = \mathrm{i}\hbar\delta_{j,k}\delta_{l,m}. \quad \text{(S9)}$$

$\boldsymbol{r}_j$ and $\boldsymbol{p}_j$ are now operators and j and k are particle indices while l and m are spatial dimensional indices.

We expand out Eq. (S8) to separate out the terms describing the independent electrons,

$$H_{el} = \sum_{j \in e^-} \frac{\boldsymbol{p}_j^2}{2m} + V_{bg}(\boldsymbol{r}_j) \tag{S10}$$

We can proceed to second-quantise this single-particle part of the Hamiltonian by choosing the Bloch states that diagonalises Eq. (S10). We denote the eigenfunctions as $\Psi_{\mathbf{k},\sigma}(\boldsymbol{r}) = e^{\mathrm{i}\mathbf{k}\cdot\boldsymbol{r}}\phi_{\mathbf{k},\sigma}(\boldsymbol{r})$, where $\phi_{\mathbf{k},\sigma}(\boldsymbol{r})$ has the periodicity of the lattice. We define the field operator for the electrons, $\psi^\dagger(\boldsymbol{r}) = \sum_{\mathbf{k}} \Psi^*_{\mathbf{k},\sigma}(\boldsymbol{r}) c^\dagger_{\mathbf{k},\sigma}$, where $c^\dagger_{\mathbf{k},\sigma}$ is fermionic creation operator for electron in Bloch state with quasi-momentum $\mathbf{k}$ and spin σ. Eq. (S10) is thus diagonal in quasi-momentum space, $H_{el} = \sum_{\mathbf{k},\sigma} \epsilon(\mathbf{k}) c^\dagger_{\mathbf{k},\sigma} c_{\mathbf{k},\sigma}$, where $\epsilon(\mathbf{k})$ is the electron dispersion. As in the main text, we assume the dispersion to be

$$\epsilon(\mathbf{k}) = \frac{\hbar^2 k^2}{2m^*}, \tag{S11}$$

where m^* is the effective mass of the electrons. We also define the Fermi wavevector k_f, Fermi velocity $v_f = \hbar k_f / m^*$ and the chemical potential μ at the Fermi level $\epsilon_f = \hbar^2 k_f^2 / 2m^*$. The couplings to the transverse light fields do not affect the choice of Bloch state basis.

B. EM field Hamiltonian

The EM field can be quantised by imposing the commutation relation

$$[\mathcal{C}_{q_1}, \pi_{q_2}] = \mathrm{i}\hbar\delta_{q_1,q_2} \tag{S12}$$

We second-quantise this part of the Hamiltonian by defining $\pi_q = \text{-i}\sqrt{\frac{\hbar\omega_q}{2}}\left(b_{-q} - b_q^\dagger\right)$ and $\mathcal{C}_q = \sqrt{\frac{\hbar}{2\omega_q}}\left(b_q + b_{-q}^\dagger\right)$. ($b_{-q} = b_q$ if q refers to the cavity mode.) Eq. (S12) implies that b_q and $b_q^\dagger$ are bosonic annihilation and creation operators.

Collecting everything together, we arrive at the quantised Hamiltonian for the 2D mobile

electrons and the electromagnetic field (which is second quantised) in Coulomb gauge,

$$H = \sum_{j\in e^-}\Big[\frac{\Big(\boldsymbol{p}_j + e\sum_q \sqrt{\frac{\hbar}{2\epsilon_0\epsilon_r\omega_q}}\boldsymbol{u}_q(\boldsymbol{r}_j)(b_q + b_{-q}^\dagger) + e\mathbf{A}_d\cos(\omega_L t)\Big)^2}{2m} + V_{bg}(\boldsymbol{r}_j)\Big] + \frac{1}{2}\sum_{\substack{j\neq k\\ j,k\in e^-}}\frac{e^2}{4\pi\epsilon_0\epsilon_r|\boldsymbol{r}_j - \boldsymbol{r}_k|} + \sum_q \hbar\omega_q(b_q^\dagger b_q + \frac{1}{2}). \quad \text{(S13)}$$

This Hamiltonian describes the full light-electron system. If we ignore the environment modes (we justify this in the next section) we arrive at Eq. (1) in the main text.

II. LIGHT-MATTER INTERACTION

In this section, we discuss the interactions between matter and the cavity and the laser light modes in Sec. II A and II B. we proceed to consider the light-matter interaction without the environment modes. We justify this in Sec. II C, where we discuss the inelastic scatterings of the laser photons into the environment modes. The scatterings heat the electrons but the effect is insignificant due to the small detuning to cavity frequency ratio and the strong cavity mode volume compression.

By expanding out Eq. (S13) and limiting q to only the cavity mode, we obtain the different transverse light field-matter interactions: paramagnetic interactions,

$$H_{para-c} = \sum_{j\in e^-}\frac{e}{m}\boldsymbol{p}_j\cdot\hat{\boldsymbol{e}}_y\sqrt{\frac{\hbar}{\mathcal{V}_c\epsilon_0\epsilon_r\omega_c}}2\cos(q_0x_j)\left(b + b^\dagger\right) \quad \text{(S14)}$$

$$H_{para-d} = \sum_{j\in e^-}\frac{e}{m}\boldsymbol{p}_j\cdot\mathbf{A}_d\cos(\omega_L t) \quad \text{(S15)}$$

and diamagnetic interactions,

$$H_{dia-c} = \sum_{j\in e^-}\frac{e^2}{2m}\frac{\hbar}{\mathcal{V}_c\epsilon_0\epsilon_r\omega_c}4\cos^2(q_0x_j)\left(b + b^\dagger\right)^2 \quad \text{(S16)}$$

$$H_{dia-d} = \sum_{j\in e^-}\frac{e^2}{2m}\mathbf{A}_d\cos(\omega_L t)\cdot\mathbf{A}_d\cos(\omega_L t) \quad \text{(S17)}$$

$$H_{dia-cd} = \sum_{j\in e^-}\frac{e^2}{m}\sqrt{\frac{\hbar}{\mathcal{V}_c\epsilon_0\epsilon_r\omega_c}}2\cos(q_0x_j)|\mathbf{A}_d|\cos(\omega_L t)\left(b + b^\dagger\right) \quad \text{(S18)}$$

A. Paramagnetic interactions

H_{para-c} describes the paramagnetic interactions between the electrons and the cavity modes. We get the interaction Hamiltonian of the form $H_{para-c} = \sum_{\mathbf{k},\sigma,\mathbf{q}} g_{\mathbf{k}}^{para-c}/\sqrt{\mathcal{S}} c_{\mathbf{k},\sigma}^{\dagger} c_{\mathbf{k}-\mathbf{q},\sigma}(b+ b^{\dagger})$, where $\mathbf{q} = \pm q_0 \mathbf{e}_x$. $\mathcal{S} \propto 1/\omega_c^2$ is the cavity area in the xy-plane. The proportionality constant is obtained using values of electron density and number of electrons from Ref. [S3]. The matrix elements evaluate to $g_{\mathbf{k}}^{para-c}/\sqrt{\mathcal{S}} \sim \frac{\hbar|\mathbf{k}|e}{m^*}\sqrt{\frac{\hbar}{\Lambda \mathcal{V}_c \epsilon_r \epsilon_0 \omega_c}}$ for $|\mathbf{k}| \gg q_0$.

We'd like to draw attention to the fact that the paramagnetic coupling strength is inversely proportional to the effective mass rather than the bare electron mass [S4]. We thus learn that this interaction is weaker for less mobile electrons.

In the rotating frame of the driving laser these interactions are time-dependent: they rotate at $\pm\omega_L$. In Ref. [S5], it is shown that the strength of the effective (current-current) interactions between electrons due to the paramagnetic interactions are $\sim g_{\mathbf{k}}^{para-c} g_{\mathbf{k}'}^{para-c}/\hbar\omega_c \mathcal{S}$.

We compare these paramagnetic interactions to the stimulated diamagnetic scatterings discussed below and note that the two interaction terms in Eq. (S14) and Eq. (S18) coincide once one switches $\mathbf{p}$ with $e\mathbf{A}_d$. Hence, we obtain an expression for the critical intensity for the driving laser, $I_{c,1}$ (corresponding to a critical magnitude for vector potential for the driving field, $|\mathbf{A}_d|_{c,1}$), beyond which the paramagnetic interactions are weaker than the stimulated diamagnetic interactions: $e|\mathbf{A}_d|_{c,1} \sim |\langle \mathbf{k}_F|\mathbf{p}e^{-i\mathbf{q}\cdot\boldsymbol{r}}|\mathbf{k}_F + \mathbf{q}\rangle| \sim \frac{m}{m^*}\hbar k_F$ for $|\mathbf{q}| \ll k_f$.

$$I_{c,1} \sim \left(\frac{m}{m^*}\right)^2 \frac{\hbar\omega_L^2\sqrt{\epsilon_r} n_e}{2\alpha}, \tag{S19}$$

where α is the fine structure constant and n_e is the electron density per unit area.

H_{para-d} does not cause electron scatterings for a one-band system since the driving field carries no momentum in the xy-plane. When there are strongly detuned electronic bands, H_{para-d} gives rise to vertical (interband) virtual transitions and the electronic bands gain momentum-dependent shifts known as dynamical Stark shifts, whose magnitudes are inversely proportional to the detunings between the driving frequency and the electronic band gap [S6]. We here assume that this detuning is sufficiently large for us to neglect the change to the electronic band of interest.

B. Diamagnetic interactions

H_{dia-c} describes the diamagnetic interactions involving only the cavity modes. These interactions scatter electrons and also shift the electron dispersions due to the term proportional to $(e^2/m)(\hbar/\mathcal{V}_c\epsilon_0\epsilon_r\omega_c)\left(2b^\dagger b+1\right)\sum_{\mathbf{k}} n_{\mathbf{k}}$. The other terms involves operators like $b^\dagger b^\dagger$ and bb, so they are also rapidly rotating (at $\pm 2\omega_L$) in the co-rotating frame of the driving laser and contribute terms of the order $\mathcal{O}(1/2\omega_L)$.

In order to neglect this diamagnetic interaction term when the cavity is not populated (as is the case in the main text), the cavity field's vacuum fluctuations shouldn't be larger than the driving field. Thus, we can estimate another critical intensity, $I_{c,2}$ (corresponding to a critical magnitude for vector potential for the driving field, $|\mathbf{A}_d|_{c,2}$) beyond which we can neglect the diamagnetic scatterings between only cavity photons: $|\mathbf{A}_d|_{c,2} \sim \sqrt{\frac{\hbar}{\Lambda\lambda^3\epsilon_0\epsilon_r\omega_c}}$

$$\implies I_{c,2} \sim \frac{\hbar\omega_L^2 c}{\Lambda\sqrt{\epsilon_r}\omega_c\lambda^3} \tag{S20}$$

H_{dia-d} is a sinusoidally oscillating constant and does not alter the electronic or the photonic states because the laser photons carry no in-plane momentum. We have again assumed that other electronic bands are so far detuned that we can neglect vertical transitions.

H_{dia-cd} describes stimulated diamagnetic scatterings described in the main text. In the rotating frame of the driving field, we ignore the rapidly rotating (at $\pm 2\omega_L$) terms in this interaction Hamiltonian (rotating-wave approximation). The time-independent terms are presented in main text Eq. (2).

We conclude that the stimulated diamagnetic interactions compete with paramagnetic scatterings with the cavity photons as well as with diamagnetic scatterings involving only the cavity fields and that they can be estimated to dominate above a critical field intensity

$$I_{cr} \sim \max\Big\{I_{c,1}, I_{c,2}\Big\} = \max\Big\{\left(\frac{m}{m^*}\right)^2 \frac{\hbar\omega_L^2\sqrt{\epsilon_r}n_e}{2\alpha}, \frac{\hbar\omega_L^2 c}{\Lambda\sqrt{\epsilon_r}\omega_c\lambda_0^3}\Big\}. \tag{S21}$$

In low-terahertz frequency range ($\sim$ 0.1THz), the critical intensity is $\sim$ 50 kWcm^{-2} (the parameters used are those used in Fig. 2(b) of the main text). The critical intensity, I_{cr} is almost always $I_{c,1}$, given by the paramagnetic scattering strength with the cavity modes. For materials with higher electron density and lower effective mass, the critical intensity increases.

C. Effect of the environment modes

The main effect of the environment light modes is the heating of the electrons through inelastic diamagnetic scatterings. We denote the corresponding interaction vertex strength $\eta_{\mathbf{q}_e}$ (its evaluation is the same as diamagnetic scattering involving the laser field and the cavity field). In this process a laser photon scatters with an electron which transitions from quasi-momentum state $|\mathbf{k}\rangle \to \left|\mathbf{k}+\mathbf{q}_\parallel\right\rangle$, into the outgoing photon is in the environment mode whose in-plane momentum is $-\mathbf{q}_\parallel$ and energy is $\left(\hbar\omega_L + \epsilon(\mathbf{k}) - \epsilon(\mathbf{k}+\mathbf{q}_\parallel)\right)$. Since the photon momenta are very small, $\epsilon(\mathbf{k}) - \epsilon(\mathbf{k}+\mathbf{q}_\parallel) \ll \hbar\omega_L$. Fermi's golden rule gives us the total scattering rate of an electron in state $|\mathbf{k}\rangle$ by this process,

$$\begin{aligned}\Gamma_{\mathbf{k}} &= \frac{2\pi}{\hbar}\sum_{\mathbf{q}_e=(\mathbf{q}_\parallel,q_z)} |\eta_{\mathbf{q}_e}|^2 \delta(\epsilon(\mathbf{k}-\mathbf{q}_\parallel) + \hbar\omega_{\mathbf{q}_e} - \epsilon(\mathbf{k}) - \hbar\omega_L) \\ &\approx \frac{2\pi}{\hbar}\sum_{\mathbf{q}_e}\left(\frac{e^2}{m}|\mathbf{A}_d|\sqrt{\frac{\hbar}{\mathcal{V}\epsilon_0\epsilon_r\omega_L}}\cos\theta_{\mathbf{q}_e}\right)^2 \delta(\hbar\omega_{\mathbf{q}_e} - \hbar\omega_L) \\ &= \frac{64\pi^3}{3}\frac{1}{\lambda_L^2}\frac{1}{\omega_L}\frac{\alpha^2\hbar I_d}{\epsilon_r m^2\omega_L^2}. \end{aligned} \tag{S22}$$

Here, $\theta_{\mathbf{q}_e}$ is the polar angle of $\mathbf{q}_e$. In our set up $\frac{\hbar\Gamma_{\mathbf{k}}}{V^{(0)}/\mathcal{S}} \sim \frac{\delta_c}{\omega_L}\Lambda$, where $V^{(0)}/\mathcal{S}$ is as defined in the main text. Therefore, when the cavity mode volume compression is significant, this inelastic scattering is much weaker than the coherent electron interactions. We can further reduce the heating effect from inelastic scattering by increasing ω_L while keeping δ_c constant.

III. ESTIMATES OF LASER INDUCED HEATING

Two potential sources of heating can be distinguished, the direct heating of the two-dimensional electron gas, which we discuss in the main text, and the indirect heating through absorption in the underlying substrate structure.

The heating rate due to the former process is negligible. We can estimate this by considering the inelastic electron scattering rate due to the environmental modes that we considered above and the maximum energy gain of an intraband scattering event for an electron. At 10THz driving frequency, and 1GW/cm^2 intensity, the heating rate is of order pW.

To discuss the importance of the second process, we consider the case of the two-dimensional electron gas at the $LaAlO_3/SrTiO_3$ interface. Currently, no continuous wave

THz sources are able to offer irradiances of 1GW/cm^2 at 10THz central frequency and an experimental realization of our proposal should consider a driving protocol based on short pulses where peak intensities exceeding 1GW/cm^2 can be easily obtained [S7]. Importantly, even upon pulsed driving, changes in the transport properties of the two-dimensional electron gas could be tracked with on-chip time-resolved conductivity measurements [S8].

In the following, we estimate the heating of a bulk $SrTiO_3$ substrate driven with 1ps long pulses at 10THz central frequency. We omit the absorption in the $LaAlO_3$ layer which is typically only few unit cells thick and model the energy deposited by the drive as:

$$E(z) = (1-R)\frac{\mathcal{F}}{d_{pump}} \exp\left\{-\frac{z}{d_{pump}}\right\}, \tag{S23}$$

where $R = 0.995$ is the reflectivity of $SrTiO_3$ at the excitation frequency [S9], $d_{pump} = 0.68\mu m$ is the intensity penetration depth of the pump, and $\mathcal{F}$ is the excitation energy density chosen to be 0.1 and 1mJ/cm^2 to reach peak intensities of 100MW/cm^2 and 1GW/cm^2 respectively.

The temperature profile $T_f(z)$ inside the sample is related to the deposited energy density $E(z)$ by the following integral equation:

$$E(z) = \int_{T_i}^{T_f(z)} C_p(T)\,\mathrm{d}T \tag{S24}$$

where $T_i = 0.5$K is the initial temperature of the sample and $C_p(T)$ is the specific heat of $SrTiO_3$ taken from an interpolation of an equilibrium measurement [S10]. As heat diffusion, happens on much longer time scales [S11] than the few picoseconds time interval in which an experiment would be performed, it was not included in these calculations.

Fig. 1(a) shows the result of these estimates. We observe that at driving peak intensities of 1GW/cm^2 the final temperature at the surface of the $SrTiO_3$ substrate has increased to $\sim$ 15K. Reducing the driving strength to 100MW/cm^2 helps to contain the heating to no more than a few Kelvins. The final temperature could be lowered even further if substrates that offer more transparency at the driving frequency are chosen.

As an example, we repeat the same calculations on a substrate featuring a 50 times longer penetration depth . The results are shown in Fig. 1(b). In this case the heating for both driving intensities is negligible. We envision that this setting could be achieved by exploiting two-dimensional electron gases at the interface with different substrate materials (as for example diamond or silicon) that offer complete transparency at the driving frequency.

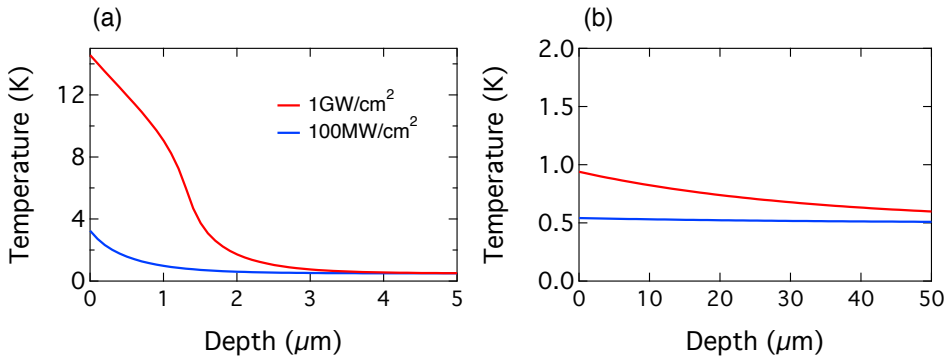

Supplemental Information, Figure 1. (a) Depth resolved temperature profiles in the $SrTiO_3$ substrate after excitation with 1ps pulses at 10THz central frequency for two different peak intensities of 1GW/cm^2 (red curves) and 100MW/cm^2 (blue curves). (b) Same calculations performed for a substrate offering a 50 times longer light penetration depth at the driving frequency.

IV. SCREENING

Here we provide details of the screening calculations in the random-phase approximation, which takes into account of all the simple bubble diagrams (See Fig. 2).

Following [S12], the RPA screened cavity-mediated interaction is

$$V^{RPA}(\mathbf{q}, i\nu_n) = |g^{RPA}(\mathbf{q}, i\nu_n)|^2 D^{RPA}(\mathbf{q}, i\nu_n) \tag{S25}$$

$$g^{RPA}(\mathbf{q}, i\nu_n) = \frac{g_0}{1 - V_c(\mathbf{q})\chi_0(\mathbf{q}, i\nu_n)} \tag{S26}$$

$$D^{RPA}(\mathbf{q}, i\nu_n) = \frac{D^{(0)}(\mathbf{q}, i\nu_n)}{1 - |g_0|^2 D^{(0)}(\mathbf{q}, i\nu_n) \frac{2\chi_0(\mathbf{q}, i\nu_n)}{1 - V_c(\mathbf{q})\chi_0(\mathbf{q}, i\nu_n)}} \tag{S27}$$

Here $V_c(\mathbf{q}) = \frac{e^2}{2\epsilon_0 \epsilon_r q}$ is the Coulomb interaction in momentum space, and χ_0 is the polarizability due to the mobility of the two-dimensional electron gas. The fraction in the denominator of Eq. (S27) is the χ^{RPA} in the main text. Note that it differs by a factor of 2 from the definition in Ref. [S12] because the scatterings with the cavity mode do not conserve total electron and photon momenta and the simple polarization bubbles connected by Coulomb interactions (which conserve total electron momentum) can be carrying $+/-\hbar\mathbf{q}$ of momentum.

$D^{(0)}(\mathbf{e}_x q_0, i\nu_n)$ is the bare cavity photon Green's function in the rotating frame for photon wavevector, $\mathbf{e}_x q_0$, and Matsubara frequency, $i\nu_n$. It reads

$$D^{(0)}(\mathbf{e}_x q_0, i\nu_n) = \frac{-2\delta_c/\hbar}{\nu_n^2 + \delta_c^2}, \tag{S28}$$

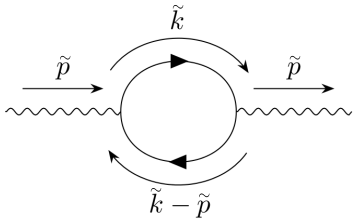

Supplemental Information, Figure 2. A simple bubble diagram. The solid lines with triangular arrows represent the bare electron Green's functions. They form a closed bubble which physically means a electron-hole pair is created and then destroyed. The wavy lines are of bosonic nature and can represent either bosonic Green's functions or Coulomb interactions. We have used 4-vector notation: $\tilde{p} = \{\mathbf{p}, ip_n\}$.

We account for the cavity decay rate by including it in the bare photon Green's function

$$D^{(0)}(\mathbf{e}_x q_0, i\nu_n) \to \frac{-2\delta_c/\hbar}{\nu_n^2 + \delta_c^2 + 2\delta_c\kappa \ \mathrm{sgn}[\nu_n]}. \tag{S29}$$

Here we define the cavity decay rate $\kappa = \omega_c/2Q$, where Q is the cavity quality factor.

With the parabolic electron dispersion [Eq. (S11)] the polarizability due to the two-dimensional electron gas, χ_0, can be found using results in Ref. [S13],

$$\mathrm{Re}\{\chi_0(q,\hbar\omega)\} = \frac{k_F^2 r_\omega}{\hbar\omega\pi}[-2r_q + C_-\sqrt{(r_q - r_\omega)^2 - 1} + C_+\sqrt{(r_q + r_\omega)^2 - 1}] \tag{S30}$$

$$\mathrm{Im}\{\chi_0(q,\hbar\omega)\} = \frac{k_F^2 r_\omega}{\hbar\omega\pi}[D_-\sqrt{1 - (r_q - r_\omega)^2} - D_+\sqrt{1 - (r_q + r_\omega)^2}], \tag{S31}$$

where $r_q = \frac{q}{2k_F}$, $r_\omega = \frac{\omega}{qv_F}$, $C_\pm = \mathrm{sign}(r_q \pm r_\omega)$ and $D_\pm = 0$ for $|r_q \pm r_\omega| > 1$, and $C_\pm = 0$ and $D_\pm = 1$ for $|r_q \pm r_\omega| < 1$.

For photon-mediated interactions, q is always very small ($r_q \approx 0$), ie. we are interested in the region of the phase space to the left of the red line in Fig. 3, where $r_\omega \gg 1$ for most frequencies. Thus, we focus on small r_q and large r_ω limit. In this limit, $\mathrm{Im}\{\chi_0\} = 0$ and

$$\mathrm{Re}\{\chi_0\} = \frac{k_F^2 r_\omega}{\hbar\omega\pi}\left(-2r_q + \sqrt{(r_q + r_\omega)^2 - 1} - \sqrt{(r_q - r_\omega)^2 - 1}\right) \tag{S32}$$

$$\approx \frac{k_F^2 r_\omega}{\hbar\omega\pi}\frac{r_q}{r_\omega^2 - r_q^2} \approx \frac{k_F^2 r_q}{\hbar\omega\pi r_\omega} = \frac{k_F v_F q^2}{\hbar\omega^2 2\pi} \tag{S33}$$

Thus

$$g^{\mathrm{RPA}}(\mathbf{q},\hbar\omega) = \frac{g_0}{1 - \frac{\omega_{\mathrm{pl}}^2(\mathbf{q})}{\omega^2}} \text{ and} \tag{S34}$$

$$D^{\mathrm{RPA}}(\mathbf{q},\hbar\omega) = \frac{D^{(0)}}{1 - |g_0|^2 D^{(0)}\frac{2k_F v_F q^2}{\hbar\omega^2 2\pi}/\left(1 - \frac{\omega_{\mathrm{pl}}^2(\mathbf{q})}{\omega^2}\right)}, \tag{S35}$$

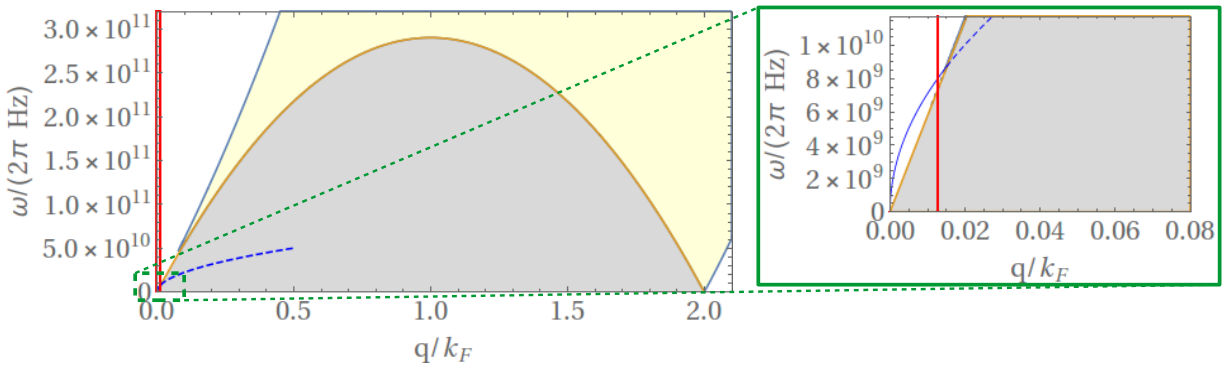

Supplemental Information, Figure 3. Phase space plot. The right figure magnifies the small dashed green box in the left figure. The mobile electron polarizability χ_0 is complex inside the shaded regions. The yellow(grey) region is where one(both) of $|r_q \pm r_\omega| < 1$. Inside both shaded regions energy can be dissipated into the electron systems through single-particle excitations. The part of phase space most relevant for the dynamics we describe is to the left of the red line. Its position corresponds to the momentum of a ≈ 1.5THz photon (which is roughly the highest cavity frequency we consider). The blue line is the 2D plasmon dispersion. Where it's dotted means the plasmons are Landau-damped. For the cavity frequencies we consider here, the bare plasmons coupled to the photons are not Landau-damped. We use the same electron parameters as those in Fig. 2(b) of the main text.

where $\omega_{\rm pl}(\mathbf{q})$ is the plasmon frequency at momentum $(\mathbf{q})$, satisfying

$$\omega_{\rm pl}^2(\mathbf{q}) = \frac{e^2}{2\epsilon_r\epsilon_0}\frac{k_F v_F q}{2\pi\hbar} = \frac{e^2}{4\pi\hbar\epsilon_0 c}\frac{k_F v_F q c}{\epsilon_r} = \frac{2\alpha}{\hbar\sqrt{\epsilon_r}}\omega_c\epsilon_F. \tag{S36}$$

We plot the plasmon dispersion in Fig. 3 for a given electron density. Note that for sufficiently large momenta the plasmons are Landau-damped, but for the parameters considered here we are not in that regime. We found that we would need cavity frequency greater than ~ 2THz in order to couple to Landau-damped plasmons. Yet this does not affect the stimulated electron interactions we describe in the paper.

In the large r_ω limit, we include electron damping by modifying the electron response function such that

$$1 - \frac{\omega_{\rm pl}^2(\mathbf{q})}{\omega^2} \to 1 - \frac{\omega_{\rm pl}^2(\mathbf{q})}{\omega^2 + \mathrm{i}\omega\gamma} \tag{S37}$$

just like in Drude model [S14, S15].

We additionally note that in addition to the attractive interaction potential shown in the

main text, a repulsive potential is achieved with blue-detuned driving. We show an example of it in Fig. 4

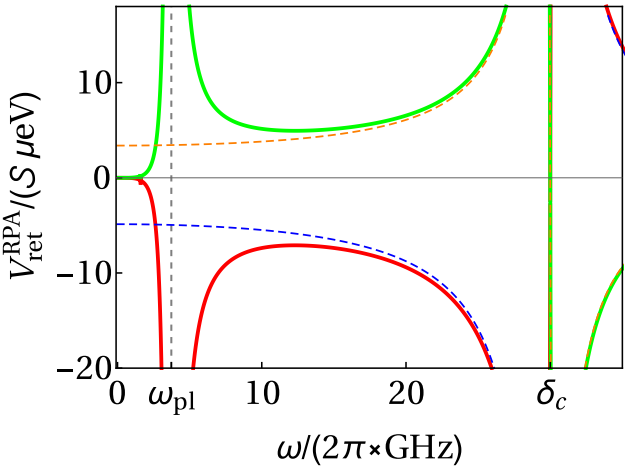

Supplemental Information, Figure 4. The real parts of the screened retarded interaction potentials for red- and blue-detuned driving are shown as red and green solid lines. The corresponding bare interaction potentials are shown with dashed curves. The vertically dashed line represents the plasmon resonance. The attractive potential curves are obtained using the same parameters as those used in Fig. 2(b) of the main text. The repulsive potential curves are obtained with the same parameters except the detuning has the opposite sign.

V. COOPER INSTABILITY

In this section, we show a calculation of the Cooper instability critical temperature by solving the Dyson equation Eq. (S38) [it comes from summing an infinite series of ladder diagrams (see Fig. 5)] [S12, S16] using the RPA screened interaction potential.

$$\Gamma(\tilde{k};\tilde{p}) = -V^{RPA}(\tilde{k}-\tilde{p}) + \frac{1}{\mathcal{S}\beta}\sum_{\tilde{q}}[-V^{RPA}(\tilde{k}-\tilde{q})]G^{(0)}(\tilde{q})G^{(0)}(-\tilde{q})\Gamma(\tilde{q};\tilde{p}) \ , \tag{S38}$$

where $\beta = 1/k_BT$, $G^{(0)} = 1/(i\nu_n\hbar - \xi_{\mathbf{q}})$ is the unperturbed electron Green's function, where $\xi_{\mathbf{q}} = \epsilon(\mathbf{q}) - \mu$.

As described in the main text we approximate the interaction potential by a δ-function

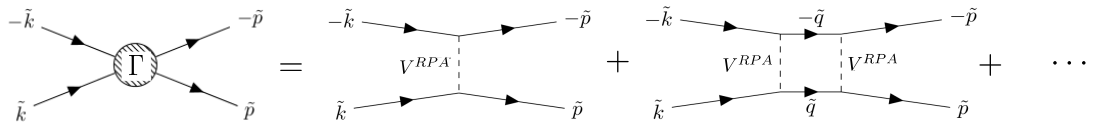

Supplemental Information, Figure 5. The pair scattering vertex Γ is given by an infinite sum of ladder diagrams of an electron pair scattering with each other repeatedly. We consider the Cooper channel, where the electrons have opposite momenta and Matsubara frequencies. The Cooper instability is signified by the divergence of this infinite sum.

in k-space. Thus, for electron states near the Fermi level the Dyson equation becomes

$$\Gamma(ik_n, ip_n) = -V^{RPA}(\mathbf{e}_x q_0 \approx 0, ik_n - ip_n) + \frac{1}{\mathcal{S}\beta}\sum_{i\nu_n}[-2V^{RPA}(\mathbf{e}_x q_0 \approx 0, ik_n - i\nu_n)]G^{(0)}(i\nu_n)G^{(0)}(-i\nu_n)\Gamma(i\nu_n, ip_n)\ . \quad \text{(S39)}$$

The factor of 2 in the sum comes from $\mathbf{q} = \pm\mathbf{e}_x q_0$. We can think of the Matsubara frequencies as indices of matrices for Γ and $\mathcal{M}(ik_n, i\nu_n) \equiv \frac{-2}{\mathcal{S}\beta}V^{RPA}(\mathbf{e}_x q_0 \approx 0, ik_n - i\nu_n)G^{(0)}(i\nu_n)G^{(0)}(-i\nu_n)$. Thus, the Dyson equation above is a matrix equation

$$\underline{\underline{\Gamma}} = -\underline{\underline{V}}^{RPA} + \underline{\underline{\mathcal{M}}}\ \underline{\underline{\Gamma}} \quad \text{(S40)}$$

and Γ diverges when $\det\left[\mathbb{1} - \mathcal{M}(\beta_c = 1/k_B T_c)\right] = 0$. The determinant tends to 1 at high temperatures and reduces as the temperature lowers.

In Fig. 6, we plot an example of the determinant as a function of temperature. Note that we introduced a cut-off for the Matsubara frequencies since high frequencies have little effect (due to $G^{(0)}$). We checked that our results do not vary when we alter the cut-off value. In fact, the factor of $G^{(0)}(i\nu_n)G^{(0)}(-i\nu_n) \propto \frac{1}{\nu_n^2}$ for fermionic Matsubara frequency $\nu_n = (2n+1)\pi k_B T/\hbar$ means that the terms in the sum with $n = -1, 0$ are almost a magnitude larger than the terms with $n = -2, 1$. Hence, a numerically quicker (and still reasonably accurate) way that we used to compute the critical temperatures in Fig. 3 is to limit the Matsubara frequencies to just $\pm\pi k_B T/\hbar$, then Eq. (S40) turns into an algebraic equation to solve:

$$1 = -\frac{2}{\mathcal{S}\beta_c}V^{RPA}(\mathbf{e}_x q_0, 2\mathrm{i}\pi/\hbar\beta_c)\frac{\beta_c^2}{\pi^2}\ . \quad \text{(S41)}$$

This method underestimate T_c only by a few percent compared to more accurate results using a higher cut-off.

Note that away from the plasmon frequency, the interaction is effectively unscreened so $V^{RPA}(\mathbf{e}_x q_0, 2\mathrm{i}\pi/\hbar\beta_c) \to |g_0|^2 D^{(0)}(\mathbf{e}_x q_0, 2\mathrm{i}\pi/\hbar\beta_c)$.

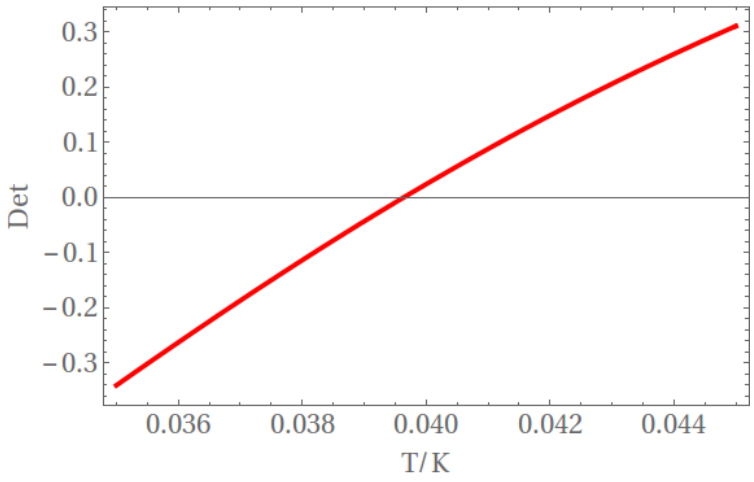

Supplemental Information, Figure 6. Determinant of $(\mathbb{1} - \mathcal{M})$ plotted as a function of temperature using the following parameters: $I_{\rm dr} \approx 6\text{MWcm}^{-2}$, $\omega_c \approx 2\pi \times 0.1\text{THz}$, $\delta_c \approx 0.05\ \omega_c$ and the same electron system parameters as in Fig. 2(b) of the main text. The point where it crosses zero is the Cooper instability critical temperature.

VI. CAVITY PHOTON NUMBER

In the equilibrium Green's function formalism, the number of bosons $N_{\mathbf{p}}$ is given by Bose-Einstein distribution, $n_B(\omega) = \frac{1}{e^{\beta\hbar\omega}-1}$, and the imaginary part of the retarded bosonic Green's function, $D_{\rm ret}(\mathbf{p},\omega)$ [S17],

$$2N_{\mathbf{p}} + 1 = \int_{-\infty}^{\infty} \frac{\mathrm{d}\omega\hbar}{2\pi} n_B(\omega)(-2\,\mathrm{Im}\{D_{\rm ret}(\mathbf{p},\omega)\}) \tag{S42}$$

In our case, we need to use the green's function in the rotated frame and an adjusted Bose-Einstein distribution,

$$n_B^{'}(\omega) = \frac{1}{\exp\left(\beta\hbar(\omega + \mathrm{sgn}[\omega]\omega_L)\right) - 1} \tag{S43}$$

to reflect that we are in the co-rotating frame. Thus, the cavity photon population is given by

$$2N_{\mathbf{p}} + 1 = \int_{-\infty}^{\infty} \frac{\mathrm{d}\omega\hbar}{2\pi} n_B^{'}(\omega)(-2\,\mathrm{Im}\{D_{\rm ret}^{RPA}(\mathbf{p},\omega)\}) \tag{S44}$$

We compute the cavity photon number by numerical integration. $D_{\rm ret}^{RPA}$ is obtained from

the Matsubara frequency formulation [Eq. (S27)] by analytic continuation $i\nu_n \to \omega + \mathrm{i}\eta$.

[S1] Mackillo Kira and Stephan W. Koch, *Semiconductor Quantum Optics* (Cambridge University Press, 2011).

[S2] Jiajun Li, Denis Golez, Giacomo Mazza, Andrew J. Millis, Antoine Georges, and Martin Eckstein, "Electromagnetic coupling in tight-binding models for strongly correlated light and matter," Phys. Rev. B **101**, 205140 (2020).

[S3] Curdin Maissen, Giacomo Scalari, Federico Valmorra, Mattias Beck, Jérôme Faist, Sara Cibella, Roberto Leoni, Christian Reichl, Christophe Charpentier, and Werner Wegscheider, "Ultrastrong coupling in the near field of complementary split-ring resonators," Phys. Rev. B **90**, 205309 (2014).

[S4] Mackillo Kira and Stephan W. Koch, "Interactions in semiconductors," in *Semiconductor Quantum Optics* (Cambridge University Press, 2011) p. 253–278.

[S5] Frank Schlawin, Andrea Cavalleri, and Dieter Jaksch, "Cavity-mediated electron-photon superconductivity," Phys. Rev. Lett. **122**, 133602 (2019).

[S6] Edbert J. Sie, James W. McIver, Yi-Hsien Lee, Liang Fu, Jing Kong, and Nuh Gedik, "Optical stark effect in 2d semiconductors," Proc. SPIE **9835** (2016), 10.1117/12.2223462.

[S7] B. Liu, H. Bromberger, A. Cartella, T. Gebert, M. Först, and A. Cavalleri, "Generation of narrowband, high-intensity, carrier-envelope phase-stable pulses tunable between 4 and 18 THz," Opt. Lett. **42**, 129–131 (2017).

[S8] J. W. McIver, B. Schulte, F.-U. Stein, T. Matsuyama, G. Jotzu, G. Meier, and A. Cavalleri, "Light-induced anomalous Hall effect in graphene," Nat. Phys. **16**, 38–41 (2020).

[S9] K. Kamarás, K.-L. Barth, F. Keilmann, R. Henn, M. Reedyk, C. Thomsen, M. Cardona, J. Kircher, P. L. Richards, and J.-L. Stehlé, "The low-temperature infrared optical functions of $SrTiO_3$ determined by reflectance spectroscopy and spectroscopic ellipsometry," J. Appl. Phys. **78**, 1235–1240 (1995).

[S10] V. Fritsch, J. Hemberger, M. V. Eremin, H.-A. Krug von Nidda, F. Lichtenberg, R. Wehn, and A. Loidl, "Magnetization and specific heat of $LaTiO_3$," Phys. Rev. B **65**, 212405 (2002).

[S11] Yasutaka Suemune, "Thermal conductivity of $BaTiO_3$ and $SrTiO_3$ from 4.5° to 300°K," J. Phys. Soc. Japan **20**, 174–175 (1965).

[S12] Henrik Bruus and Karsten Flensberg, *Many-body quantum theory in condensed matter physics - an introduction* (Oxford University Press, United States, 2004).

[S13] Frank Stern and W. E. Howard, "Properties of semiconductor surface inversion layers in the electric quantum limit," Phys. Rev. **163**, 816–835 (1967).

[S14] Mark Fox, *Optical properties of solids*, Vol. Oxford master series in condensed matter physics (Oxford University Press, 2001).

[S15] Charles Kittel, *Quantum theory of solids* (John Wiley & Sons, New York, 1987).

[S16] A. A. Abrikosov, *Methods of quantum field theory in statistical physics* (Dover Publications, New York, 1975).

[S17] G.D. Mahan, *Many-Particle Physics*, Physics of Solids and Liquids (Springer US, 2000).